Ionic conductivity of solid polymer electrolytes depending on elongation

Roselyne Jeanne-Brou, Nicolas Charvin, Gilles De Moor, Lionel Flandin, Sébastien Issa, Trang N.T. Phan, R. Bouchet, Didier Devaux

Ionic conductivity of solid polymer electrolytes depending on elongation

Roselyne Jeanne-Brou[1], Nicolas Charvin[1], Gilles de Moor[1], Lionel Flandin[1], Sébastien Issa[2], Trang N. T. Phan[2], Renaud Bouchet[1,], Didier Devaux[1,**]**

[1] Univ. Grenoble Alpes, Univ. Savoie Mont Blanc, CNRS, Grenoble INP[*], LEPMI, 38000 Grenoble, France.

[*]Institute of Engineering and Management Univ. Grenoble Alpes

[2] Aix Marseille Univ., CNRS, Institut de Chimie Radicalaire-UMR 7273, Marseille, France.

[**]Corresponding author: renaud.bouchet@grenoble-inp.fr, didier.devaux@cnrs.fr

Abstract

Research on solid polymer electrolytes (SPEs) based on poly(ethylene oxide) (PEO) is essential to propose an alternative to the conventional liquid electrolyte in order to increase both the mechanical properties and the ionic conductivity. Strategies to increase the ionic conductivity of SPEs are typically based on the development of new polymer architectures, lithium salt natures, plasticizers, or additives. In addition, applying an external field such as magnetic, electric, pressure, or a mechanical deformation onto the SPEs can alter the resulting ionic transport properties. For the later one, the main difficulty lies in obtaining the instantaneous evolution of the ionic conductivity coupled with the mechanical deformation and its geometrical change, especially when a striction domain appears. For this, a dedicated sample environment was designed to perform tensile tests in an inert atmosphere on SPE membranes at different temperatures (below and above the PEO melting temperature). Moreover, a methodology to calculate the instantaneous in-plane ionic conductivity is proposed based on COMSOL simulations to back out the sample geometrical changes during elongation. A strong impact on the in-plane ionic conductivity is observed when comparing PEO electrolyte architectures; from homopolymers to single-ion conducting block copolymer via binary conducting block copolymer electrolytes. Below the PEO melting temperature, a striction domain appears upon elongation whose conductivity is higher than the one of the bulk by a factor 2 and 18 for PEO homopolymer and binary conducting block copolymer electrolytes, respectively.

Keywords: solid polymer electrolyte, anisotropy, ionic conductivity, stretching, in situ measurements.

1. Introduction

Existing Li-ion battery technologies are limited for large scale application because of the presence of flammable liquid electrolytes (lithium salt in alkyl carbonate solvents).[1] The solid polymer electrolytes (SPEs) based on polyethylene oxide (PEO) directly address this issue, but present a relatively low ionic conductivity (σ) at temperatures below the melting point (T_m) of about 55 °C with value typically lower than 10^{-5} S.cm^{-1}. Thus, the operating temperature is typically increased up to 60 - 80°C to achieve the required conductivity, above 10^{-4} S.cm^{-1}, for the application.[2] Therefore, there is a need to favor ionic transport in the SPE below 60 °C to move toward a room temperature application. For example, the addition of micro or nanoparticles in a polymer matrix helps to increase the mechanical properties and to decrease the crystallinity of the PEO phase.[3] In addition, the ionic conductivity differs depending on the nature of the SPE such as homopolymer, copolymers, crosslinked polymers, or single-ion conducting electrolytes.[4–6] It has also been reported that SPEs possess an anisotropic ionic conductivity where the in-plane differs from the through-plane conductivity depending on the SPE architecture and the orientation of the polymer chains (e.g. linear, diblock, triblock or branched copolymers).[5,7] Moreover, this anisotropy can be further exacerbated by structuring the materials with the application of either an electrical or magnetic external field [8] during the solvent drying step[9] or by controlling the drying temperature.[10] At last, the application of a mechanical strain is also known to modify the electrical properties in homogeneous or heterogeneous systems.[11–16]

Golodnisky and Peled pioneered the study of the SPE elongation under uniaxial stress.[11,17] For instance, they compared the ^{7}Li nuclear magnetic resonance (NMR) spectra of unstretched and stretched PEO/LiI films at room temperature. In the stretched SPE, the chemical shift upfield is consistent with a closer Li-O bond lengths where the PEO takes the form of a helix with the -O atoms located inside and complexing the cations while the -H atoms are facing outward. These changes within the microstructure are reversible by heating the samples above T_m, the peak positions measured at room temperature returned to that of the unstretched state. This results from the relaxation of the polymer chains that return to a Gaussian state. Additional studies focused on the influence of temperature, stretching, polymer chain structure (microscopy study), and Li salt concentration on the in-plane and/or through-plane ionic conductivity of PEO homopolymer electrolytes.[11,14,18,19] For high molecular weight PEO membranes doped with LiI (EO/Li = 20), Golodnitsky *et al.* reported that stretching up to 150 % at room temperature leads to an increase in the in-plane

conductivity by a factor 4 to 7.[11,18,20] When changing salt with LiTFSI, the in-plane conductivity was enhanced by a factor 10 at an elongation of about 450 %.[19] Typically, stretching the electrolytes in their plastic domain leads to an increase in the in-plane conductivity. This phenomenon has been ascribed to the morphological changes that occur during the non-reversible deformation.[13] With increasing deformation, the crystalline grains start to slide and align with the direction of the applied load. When the stress reaches a critical point that marks the beginning of yielding, dislocation density rises in the favorably oriented crystalline grains that experience excessive shear, leading to the formation of fibrils.[13] Liu *et al.*[21] measured the in-plane conductivity at 25°C of PEO/LiTFSI and PEO/$LiCF_3SO_3$ films before and after their stretching at 90 °C under dry air flow. They reported a decrease in conductivity by a factor of 0.6 and 0.7 at 200 and 300 % of elongation, respectively. They attributed this loss in conductivity to a modification of the PEO crystalline phase after the stretching step that tends to adopt an orientation perpendicular to the stretching direction and thus block in-plane ionic pathway. Conversely, in through-plane direction, the conductivity increases in correlation with a reduced tortuosity. However, these results contradict the works of Burba *et al.*[22] where the stretching at room temperature of high molecular weight PEO/LiTFSI is enhanced in a direction parallel to the stretched direction which indicate that the stretching temperature, and thus the polymer state, plays a key role on the resulting conductivity.

From this literature analysis (the data are summarized in **Table S1**, see supporting information file), the change induced by mechanical stretching on the in-plane ionic conductivity of PEO based electrolyte are not fully univocal. This results from the intrinsic complexity to measure the changes of conductivity upon stretching, or to the high sensitivity of small changes in the experimental conditions (dry air, ambient atmosphere, sample preparation, etc.). In addition, the dynamic changes of the in-plane conductivity at different temperatures have not been fully addressed. The relaxation mechanisms might also alter the conclusions. Finally, the PEO homopolymer is the sole material for which the conductivity has been measured upon stretching. This gives a little perspective to correlate and thereby understand the changes in conductivity upon stretching of SPEs of different natures and/or architectures. Indeed, from a practical point of view, understanding the evolution of the in-plane as well as the through-plane conductivity to get the conductivity anisotropy (ratio of in-plane over through plane conductivity), upon elongation is of interest for the solid-state battery devices as solid-state electrolytes are foreseen to be produced in industry by extrusion

process In addition, the anisotropy if understood and controlled can be used to increase the anisotropy to get low parallel values limiting the formation of longitudinal gradient which has been suggested as the origin of the dendrite nucleation even at current density far below the Sand current density.[23]

Herein, we propose to revisit the in-plane ionic conductivity analysis. To perform reliable experiments, we first developed a dedicated setup to couple electrochemical impedance spectroscopy as a function of the elongation in an inert atmosphere and at various temperatures. The measurements are performed either as a function of an on-going elongation (continuous mode) or as a function of time after a stepwise elongation (stop-motion mode). To obtain the intrinsic transport property, a methodology is presented based on the combination of the SPE geometrical dimensions extracted from optical pictures and processed with the Fiji software [24], and a finite element modeling done under COMSOL Multiphysics[25] to dynamically take into account the evolution of the SPE geometry. This leads to the determination of the cell constant as a function of the elongation. In this work, the experiments were performed at given temperature, above and below T_m of PEO, and the nature of the SPEs was varied using PEO homopolymers, polystyrene (PS) reinforced triblock copolymer (PS-PEO-PS), and a crosslinked single-ion conducting electrolytes. Below T_m, a necking region is locally generated within the semi-crystalline stretched PEO and PS-PEO-PS with higher conductivity than that of the bulk.

2. Experimental

2.1 Materials

Solid polymer electrolytes and cell assembly

Lithium bis(trifluoromethanesulfonyl)imide (LiTFSI) and high molecular weight (5000 $kg.mol^{-1}$) PEO homopolymers (PEO_{5000}) were obtained from Sigma Aldrich and used as received. Triblock copolymers with a central 20 $kg.mol^{-1}$ PEO sequence with outer blocks in Polystyrene (PS) having a PS weight fraction of 0.53, denoted $SEO_{20}S\_53$, was synthesized by nitroxide mediated polymerization at Institut de Chimie Radicalaire (Aix-Marseille Univ., France) as reported previously.[6,7] The chemical structures of the PEO and $SEO_{20}S\_53$ are shown in **Table 1**. To formulate SPE, the two polymers were blended with LiTFSI to reach a salt concentration equivalent to EO/Li of 25.[25] The polymer and salt are solubilized in a

good solvent, as N,N-dimethylformamide (DMF), and the resulting solution is casted onto a Polytetrafluoroethylene Petri dish, then let dry and annealed at 60°C prior being stored in an Argon filled glove box for at least a week prior use. Then, the SPEs were sealed in pouch bags to be further annealed at 80 °C for 4 h in an oven to remove the formulation process history [26–28] and subsequently stored again in the Argon dry glove box for at least a week prior use. The SPEs were formulated in the form of thin films with typical thicknesses ranging from 100 to 250 µm.

A crosslinked single-ion conducting electrolyte was also synthesized by Institut de Chimie Radicalaire (Aix-Marseille Univ.) based on silica nodes functionalized with TFSI anions with PEO chain in between. The generic chemical structure of this single-ion conducting SPE, denoted HySI_20 with 20 the equivalent EO/Li ratio is added in **Table 1** while the complet set of physico-chemical and ionic transport properties are reported in reference [29]. The HySI_20 film thicknesses range in between 100 to 300 µm thick, *i.e.* similar to the PEO and SEO_{20}_53 electrolytes.

At last, for comparison purpose, a 49 ± 1 µm thick commercial (Osaka Soda) crosslinked PEO-based electrolyte denoted PEO_{OS} was also used to validate our methodology.[30]

Acronym	Chemical representation
PEO_{5000}	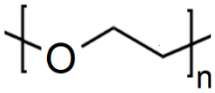
$SEO_{20}S\_53$	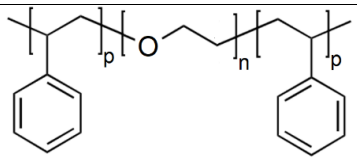
HySI_20	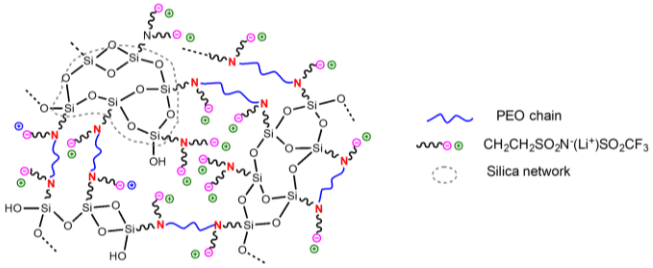

Table 1. Chemical structure of the investigated polymer hosts, PEO_{5000} and $SEO_{20}S\_53$ that are doped with LiTFSI (EO/Li = 25), and of the HySI_20 crosslinked single-ion conducting electrolyte.

In the glove box, each SPEs were cut in the form of a rectangle or a dumbbell using hand punchers whose typical dimensions are shown in **Figure S1**. These form factors are being designed for in-plane impedance measurement as electrodes can be placed on both ends of the materials. We thus define as *L* the distance in between the two electrodes.

2.2 Sample environment

A sample environment was specifically designed to perform in-plane electrochemical impedance spectroscopy of the investigated SPEs depending on the strain (ε) and temperature (T) under a control atmosphere (constant Nitrogen (N_2) flow). The sample environment is schematized using Solidworks[31] in **Figure 1a** and a camera picture is displayed in **Figure 1b**. It consists in a Minimat 2000 tensile device that was modified to only keep the parts necessary for uniaxial elongation. These parts correspond to the clamp, endless screws to apply the strain, and the mechanical coupler to an external stepper-motor. In addition, the clamps were elevated above the screws to be able to measure the SPE thickness with a micrometer or its width as illustrated in **Figure S2**. Moreover, the clamps were insulated with Kapton tape, and a rectangular Cu tape was placed in each of them to act as electrodes, *i.e.* a Cu symmetric in-plane cell. The whole system was placed in a closed plastic box from FIBOX Enclosing Innovation that can withstand up to 200 °C. It was partially covered with a heat resistant and thermal insulating tape to help control the temperature in the box, leaving a small open window to visualize the sample during elongation tests; enabling to take pictures of the SPE sample for geometric corrections. A heater and a fan were also added into the box, to enable temperature control via a thermocouple placed close to the SPE sample. In addition, a stepper motor was connected to the Minimat to control the moving-clamp displacement in both directions to widen or close the gap between the clamps. The speed was set to 1 $mm.min^{-1}$ (minimum possible) and no force sensor was installed. When the box was closed, inert N_2 gas was flown via two openings (inlet and outlet) placed on both ends. To mount a SPE, both ends of a sample were placed on the Cu electrode in each clamp that was subsequently close at 5 cN.m using a torque screwdriver. This value is the best trade-off ensuring good electrical contacts of the SPE with the electrodes (to get reliable EIS spectra) and preventing the membrane from breaking. Then, electric wires, indicated by the white arrows in **Figure 1b**, enables the connection from the Cu electrodes to a potentiostat with impedance capability (SP200, BioLogic) via electric connectors placed on the box wall. The complete setup is displayed in **Figure S3** where the sample environment is placed vertically, and a camera is placed in front of the opening to capture images of the SPE.

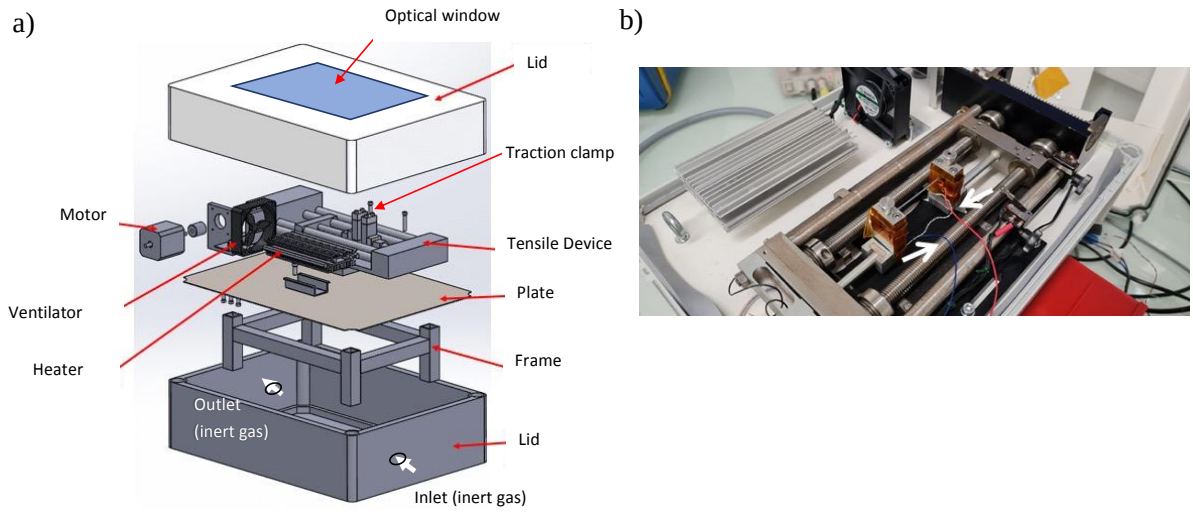

Figure 1. a) SolidWorks rendering of the sample environment for the in-plane impedance analysis as a function of the strain, b) picture of the sample environment comprising a SPE placed in between the clamps and the wire connection to the potentiostat.

2.3 Camera picture analysis

A Digital Single-Lens Reflex (DSLR) camera with a zoom lens (Nikon) was used to acquire pictures of the SPE surface upon elongation which was controlled remotely to prevent vibration and measure the width and the length (see **Figure S3**). As an example, a picture of the HySI_20 electrolyte held in between the clamps is shown in **Figure S4**. For each picture, the SPE is outlined using the Fiji software and the pixel size is defined using a millimeter graph paper acting as a sight and located at the level of the SPE. The distance between the electrodes (L) is thus the sum of the pixels in between the clamps while the projected surface area (A) is the number of pixels within the outlined surface. Therefore, we define the averaged width (w_{avg}) as:

$$w_{\mathrm{avg}} = \frac{A}{L} \tag{1}$$

2.4 Electrochemical impedance spectroscopy

Using the sample environment, at a given temperature (T) and under constant flow of N_2 gas, electrochemical impedance spectroscopy (EIS) was performed during SPE elongation in working to ground mode to avoid interference from the heating power source with the cell potential. EIS spectra were recorded from 7 MHz down to 20 mHz using an excitation signal

between 500 and 1500 mV. **Figure 2a** shows an example of EIS spectrum of the HySI_20 electrolyte after temperature equilibrium at 35 °C. Because of the cell geometry with a large SPE length, the impedance is very high and an electrical equivalent circuit made of the electrolyte resistance (R_{el}) in parallel with a pseudo-capacitance (Constant Phase Element, CPE_{el}), shown in the inset of **Figure 2a**, permit to fit the spectra.[32] The result of the best fit is added in **Figure 2a**. In addition, a Bode representation of the impedance modulus ($|Z|$) is provided in **Figure 2b** showing that for frequencies (f) below 0.4 Hz, Re(Z) is similar to $|Z|$. This means that following Re(Z) as a function of time at f = 150 mHz permits to follow the R_{el} during elongation. Indeed, at such f an impedance data point is recorded every 15 sec, corresponding to a sample elongation of ~250 µm (< 1.5 % x L), so they are performed in quasi-stationary conditions. This protocol was validated with complete EIS spectra on different SPEs prior and at the end of elongation to determine the f range at which R_{el} should be measured. As an example, **Figure S5** shows the EIS spectrum and the Bode-like at the same SPE still at 35 °C at a 90 % elongation. Consequently, R_{el} was followed at a fixed frequency of 150 mHz during elongation at 1 mm.min^{-1} until SPE break-up for all the investigated SPEs.

For comparison purpose, aluminum (Al) symmetric pouch cells were also assembled in the glove box using similar SPE geometries (rectangle, dumbbell) following the cell assembly methodology reported elsewhere.[33] The Al symmetric cell were placed in an oven and EIS spectra were recorded in between the room temperature and 90 °C. The EIS spectra were of similar shape than the one recorded using the sample environment (**Figure 2a**) and R_{el} was thus determined using the same electrical equivalent circuit.

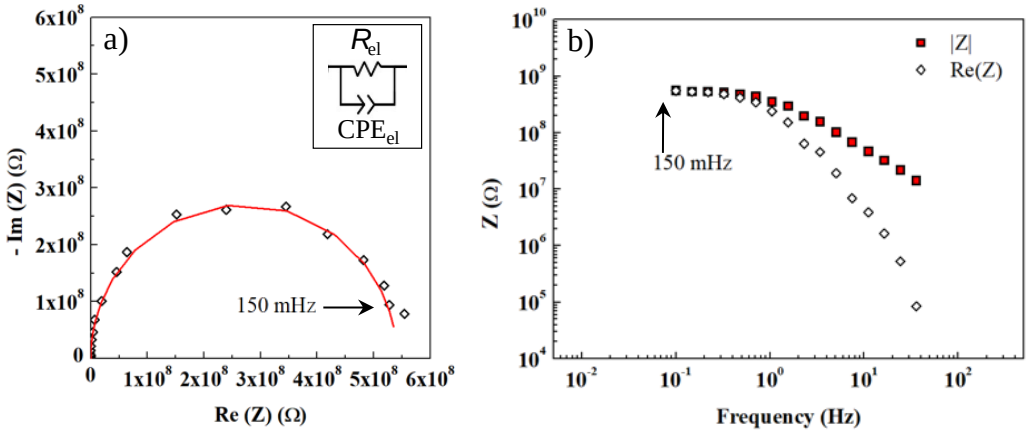

Figure 2. a) Nyquist plot of the HySI_20 electrolyte at 35 °C in initial state (ε = 0 %) with the data as open symbols and the result of the best fit from the equivalent circuit given in the inset as a red curve, b) corresponding Bode-like plot of the modulus and real part of the impedance.

2.5 Finite elements simulation

Two 3D geometries (length, width, thickness) of the SPE in the form of a dumbbell were implemented in COMSOL Multiphysics to reflect the SPE dimensions at initial state and at a given elongation. From camera pictures, the projected surface of a SPE was outlined in Fiji and an in-house Python script transforms the outlined surface in (x, y) coordinates. For the thickness, along the z-axis, a fixed value is used as input parameter corresponding to the experimental average thickness measured prior or after an elongation test using a micrometer (Mitutoyo, ± 1 µm resolution). An example such volume rendering is provided in **Figure 3** for the HySI_20 electrolyte at 0 % (332 µm thick) and 90 % (209 µm thick) of elongation along with their respective camera pictures. Then, finite element modeling was used to simulate the current distribution within the SPE volume during constant polarization in between electrodes located on both end of the samples. The complete methodology is similar to that described in a previous work for which electrodes are placed on both end of a SPE in an in-plane configuration.[25]

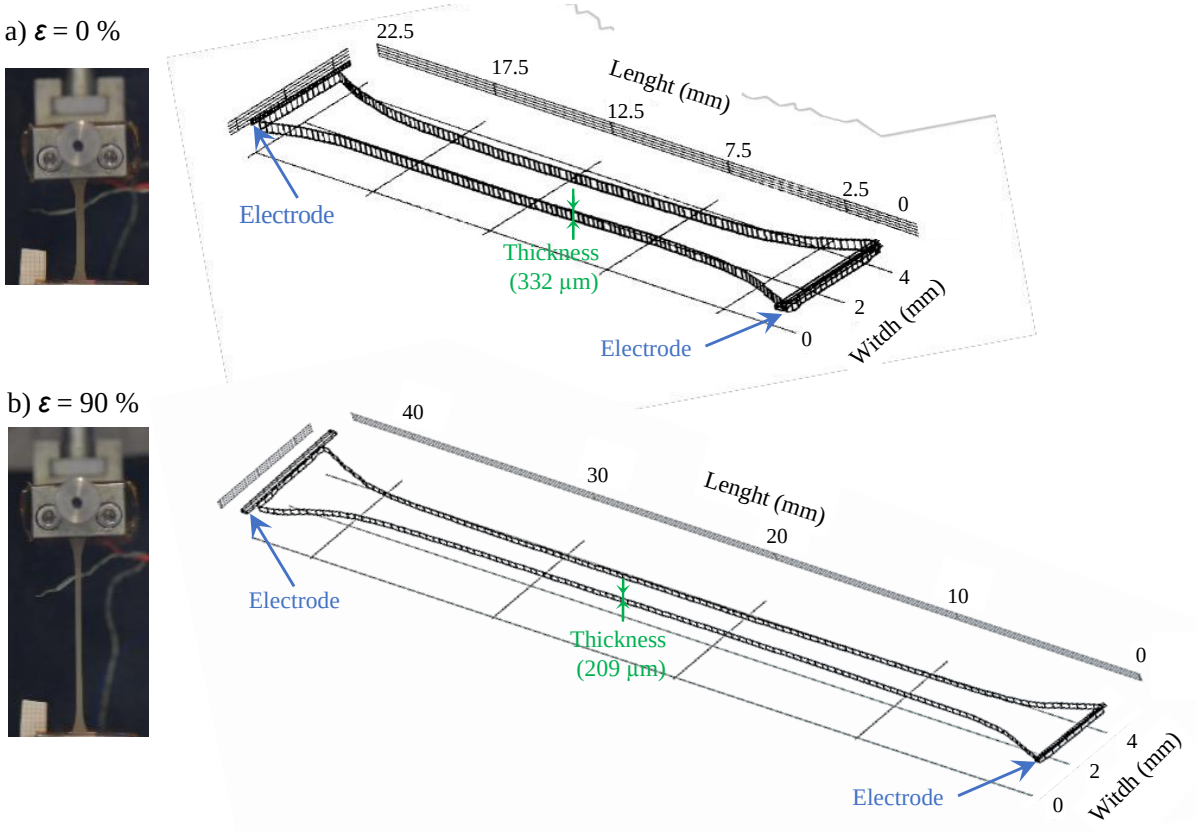

Figure 3. 3D representations under COMSOL of the HySI_20 electrolyte at an elongation (ε) of a) 0 % and b) 90 %. The positions of the electrodes on each side are also indicated as well as the corresponding camera pictures.

2.6 Thermodynamic analysis

The thermodynamic properties of the electrolytes were analyzed on a Differential Scanning Calorimetry (DSC) apparatus (DSC 2, Mettler Toledo) using several cool/heat/cool cycles from -100 °C to 125 °C and at a heating and cooling rate of 20 °C.min^{-1}. Since the sample elongation can impact their thermodynamic properties, the samples were cooled down to -100 °C prior heating them up. The heating cycles were used to determine the glass transition temperature (T_g) by the tangent lines method and from the endothermic peak the PEO melting temperature (T_m) as the intersection point of the baseline and the inflectional tangent at the beginning of the melting peak. The T_g and T_m values of the SPEs are listed in **Table S2**. In addition, for PEO homopolymer electrolyte the crystallinity index (χ_c) was calculated from the melting enthalpy (ΔH_m, determined by melting peak integration) according to:

$$\chi_c = \frac{\Delta H_m}{\Delta H_m^0} \cdot 100 \quad (2)$$

with ΔH_m^0 the melting enthalpy of a 100 % crystalline PEO, equal to 195 J.g^{-1}.[34]

2.7 Mechanical analysis

A Dynamical Mechanical Analysis (DMA) apparatus (Q800, TA Instruments) was used to perform strain-stress experiments on PEO_{5000} at 60 °C. Rectangular samples were mounted on the DMA clamps and dried for 45 min at the operating temperature via the flow of dry air in the machine. Then, the SPE was stretched at 0.5 N.min^{-1} up to 18 N or upon break-up.

3. Results and discussion

At a given elongation (ε) the in-plane ionic conductivity ($\sigma_{//}$) is determined using the conventional equation:

$$\sigma_{//} = \frac{k_{//}}{R_{el}} \quad (3)$$

with $k_{//}$ in-plane cell constant which depends on the geometrical dimensions of the SPE.

If during elongation, there is no phase transition within the SPE, then at a given ε, $\sigma_{//}$ is considered as constant in the whole sample. This hypothesis only assumes that the strain levels are comparable throughout the samples. Therefore, the SPE can be decomposed into N

small parallelepipeds of length L/N of averaged width w_{avg} and resistance R_i ($1 \leq i \leq N$) such as:

$$R_{el} = \sum_{i=1}^{N} R_i \quad (4)$$

Then, assuming a constant SPE thickness (th), eq. 4 can be written based on the in-plane conductivity of parallelepiped electrolyte[25] as:

$$R_{el} = \sum_{i=1}^{N} \frac{L/N}{w_{avg} \cdot th \cdot \sigma_{//}} \quad (5)$$

Eq. 5 can then be written in the form of eq. 3 as:

$$\sigma_{//} = \frac{L}{w_{avg} \cdot th \cdot R_{el}} \quad (6)$$

To assess on the validity of eq. 6 when the SPE is not stretched, Al symmetric pouch cells comprising a PEO_{OS} crosslinked electrolyte with a rectangular or dumbbell shape (see **Figure S1**) were assembled. This SPE was selected because this industrial product has a constant thickness. In-plane impedance measurements were then performed in between 25 and 90 °C. The pouch cells conductivities are shown as a function of the inverse of T in **Figure 4**. At each T, $\sigma_{//}$ is similar for both types of SPE geometries (rectangle and dumbbell) validating the use of eq. 6. In addition, the same SPE with a dumbbell shape was placed in the sample environment and the electrolyte was heated at selected T (40, 60 and 80 °C) under a constant N_2 flow without being stretched. From the impedance spectra of the Cu in-plane symmetric cell comprising the SPE, eq. 6 was used to calculate $\sigma_{//}$. The results are added to **Figure 4** and overlap with the other data sets. Consequently, these impedance measurements show that i) the proposed methodology to determine $\sigma_{//}$ based on the coupling of impedance with camera pictures is suitable as long as the thickness is known and ii) the atmosphere reached inside the sample environments via heated N_2 is close to that of the dry atmosphere of an Ar glove box.

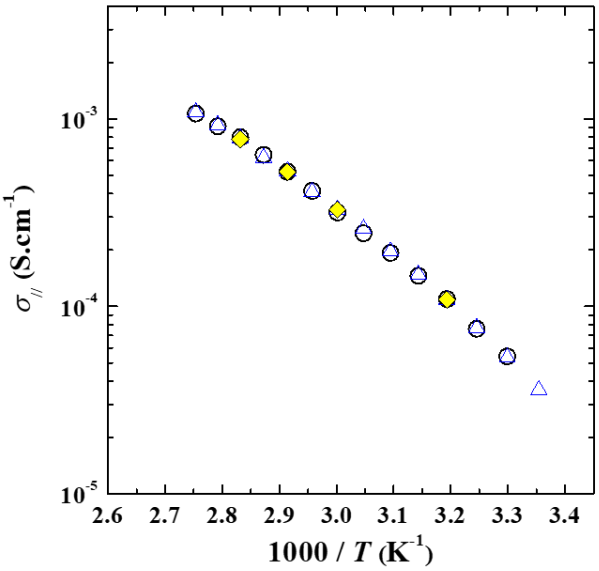

Figure 4. In-plane ionic conductivity ($\sigma_{//}$) as a function of the inverse of the temperature (T) of the PEO_{OS} electrolyte having the shape of a (black open circle) rectangle in pouch cell, (blue open triangle) dumbbell in pouch cell, and (yellow diamond) dumbbell in the sample environment.

To verify further the use of eq. 6 when a SPE is stretched, the current density (J) distribution within the electrolyte was simulated[25] on the implemented 3D geometries in COMSOL (see **Figure 3**) during a 50 mV polarization step. For this, the input parameters correspond to the experimental conductivity of the HySI_20 electrolyte of 5.83 10^{-7} S.cm^{-1} at 35 °C, called σ_{input}, and the SPE geometrical dimensions. The output parameter is J located at each node of the SPE volume. The results of the simulations are presented in **Figure 5** displaying J within the SPE (width per length) at initial state (ε = 0 %) and at a ε = 90 % with a color code ranging from dark blue (lower J) to dark red (higher J) along with camera picture of the SPE. At initial state, J is almost constant throughout the sample with values around 1.5 10^{-5} mA.cm^{-2} as the SPE is almost a parallelepiped. When stretched, J is higher in the middle of the SPE length where the width is the thinner with values around 8.1 10^{-6} mA.cm^{-2} and tends to be smaller when the width increases.

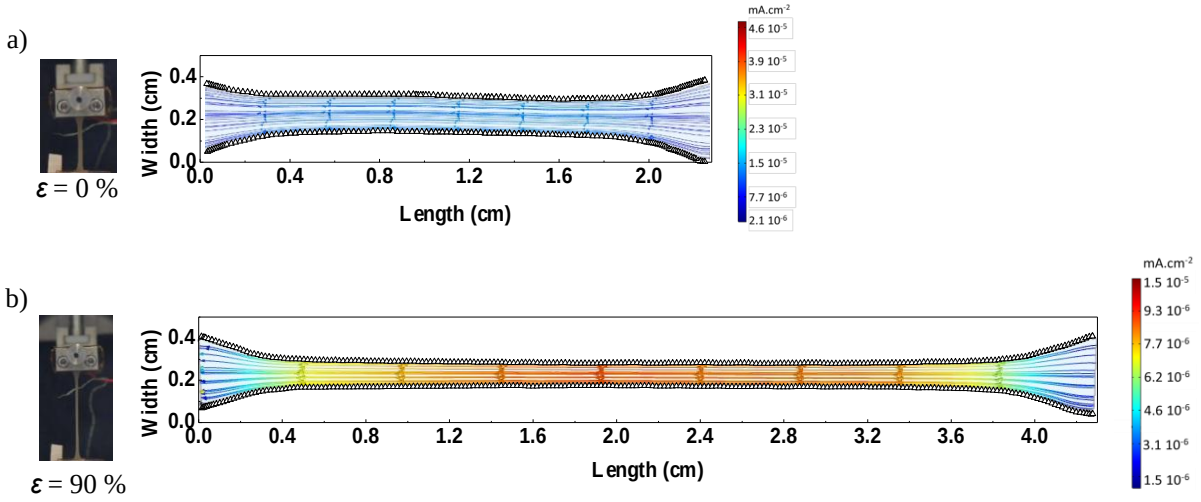

Figure 5. Current density profiles from COMSOL simulations of the HySI_20 electrolyte at a) ε = 0 % and b) ε = 90 %. The current density color code is indicated as well as the corresponding camera pictures.

The current densities were then converted into current (I) based on their usual relationship, given in eq. 7, considering a section vector $\overrightarrow{dS}$ along the SPE length:

$$I = \iint_S \vec{J}.\overrightarrow{dS} \qquad (7)$$

For completeness, **Figure S6** displays J and I as a function of the SPE length for the two elongations. The current is constant all along the SPE length with an average value of 8.48 ± 0.38 10^{-8} mA and 1.88 ± 0.05 10^{-8} mA at ε of 0 and 90 %, respectively. These values were then used to calculate the electrolyte resistance (R_{el}) based on Ohm's law (ratio E/I). The results are presented in **Table 2**. Based on eq. 6, the output $\sigma_{//}$ was calculated using the values of R_{el}, $L(\varepsilon)$, and $th(\varepsilon)$ while $w_{avg}(\varepsilon)$ was determined from Fiji analysis (eq. 1). The output $\sigma_{//}$ lies within a 5 % margin error from the input conductivity at ε = 90 %, a value lower than the typical experimental standard deviation. Therefore, this methodology based on camera picture analysis of the sample dimensions ($L(\varepsilon)$, $A(\varepsilon)$) to determine the $\sigma_{//}$ is in agreement with the results from the COMSOL simulations and can be applied experimentally for any homogeneous samples at a given elongation if the thickness is known.

ε (%)	σ_{input} (S.cm^{-1})	E (V)	L (cm)	th (µm)	A (cm²)	w_{avg} (mm)	I (A)	R_{el} (=E /I) (MΩ)	σ_{output} (eq. 6) (S.cm^{-1})
0	5.83 10^{-7}	0.05	2.28	332	0.46	1.99	8.48 ± 0.4 10^{-11}	589.6	5.80 10^{-7}
90	5.83 10^{-7}	0.05	4.30	209	0.61	0.14	1.88 ± 0.1 10^{-11}	2659.6	5.50 10^{-7}

Table 2. Results of the COMSOL simulations at 0 % and 90 % strain of a SPE.

To determine the thickness (*th*) evolution as a function of the strain, PEO_{5000}, $SEO_{20}S\_53$, and HySI_20 electrolytes were stretched at given elongations from 0 % to 115 % and at 35, 42, or 60 °C. As the sample environment is a closed box, the thicknesses are measured from SPEs quickly unmount from the clamps at different locations along their length using a micrometer to calculate an averaged value. As an example, **Figure 6** represents the normalized average thickness, $th(\varepsilon)$ / $th(\varepsilon=0)$, as a function of ε for the HySI_20 electrolyte. The normalized average thickness of the SPEs decreases with ε and all the data tend to follow a negative power law curve. To model this evolution, we propose to use the Poisson's law in the case of large elongation. The complete set of equations is presented at the end of the Supporting Information document. The SPE volume variation, $V(0) - V(\varepsilon)$, can be expressed as a function of ε and the Poisson's ratio (ν) according to:

$$\frac{V(0) - V(\varepsilon)}{V(0)} = (1+\epsilon)^{1-2\nu} - 1 \quad (8)$$

with $V(\varepsilon)$ the volume at a given elongation and $V(0)$ the initial one.

In addition, $V(\varepsilon)$ is related to the SPE area $A(\varepsilon)$ determined using the camera pictures by:

$$V(\epsilon) = A(\epsilon) \cdot th(\epsilon) \quad (9)$$

Therefore, we obtain:

$$\frac{th(\epsilon)}{th(0)} = \frac{A(0)}{A(\epsilon)}(2 - (1+\epsilon)^{1-2\nu}) \quad (10)$$

In eq. 10, the SPE thickness follows a negative power law of the elongation considering the experimental width variations. The average thickness of a sample is thus determined prior and after stretching, and the camera pictures are used to determine $A(\varepsilon)$. Then, eq. 10 interpolates the thicknesses for intermediate ε by adjusting the thickness change with a constant ν value. This protocol is determined for each data set (a SPE at a given T) and exemplified in **Figure 6**. For PEO_{5000}, a Poisson's ratio of 0.5 and 0.36 is obtained at 60 °C and 42 °C, respectively. These values agree with literature data as ν is typically of 0.5 for amorphous polymers and in between 0.3 and 0.5 for semi-crystalline material.[35] In addition, it has also been reported for a PEO/$LiClO_4$ electrolyte ν values of 0.23 and 0.32 from 18 to 25 °C.[11] When a structural

blocks is present within the SPE as in $SEO_{20}S\_53$ and HySI_20 ν is around 0.38 (see later for example **Figures 8** and **9**).

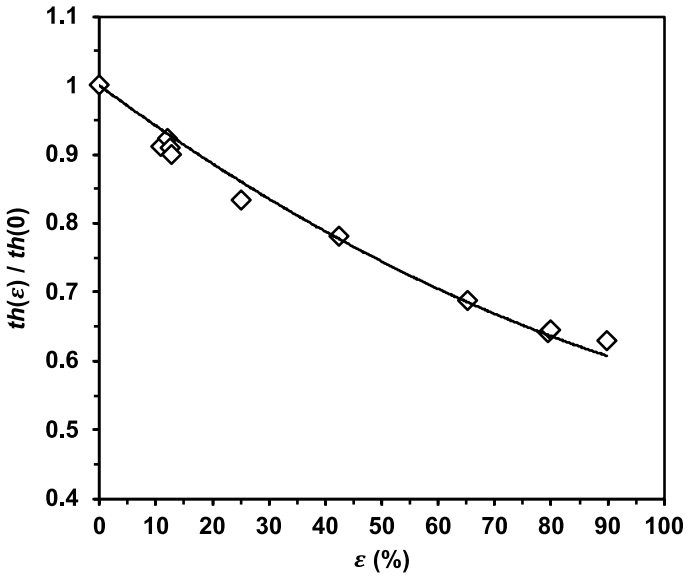

Figure 6. Normalized average thickness, $th(\varepsilon) / th(0)$, as a function of the elongation (ε) at 35 °C for the HySI_20 electrolyte from (open symbols) experimental data and (black line) interpolated data (eq. 10 with $\nu = 0.37$).

In conclusion, with this methodology, the in-plane conductivity of SPEs can be calculated as a function of the strain (ε) and the temperature (T) as the cell constant ($k_{//}$) of the sample environment takes into account the SPE geometrical deformation as long as no defect area appears in the sample.

Series of SPEs were then subjected to elongation experiments at a given T, typically 35 or 60 °C, either in continuous mode or in stop-motion mode (see experimental part). The PEO_{5000} electrolyte was first stretched at 60 °C. At such T the electrolyte is amorphous[25] as confirmed by DSC analysis (see **Table S2**) and is a viscoelastic fluid.[37] **Figure 7a** represents the evolution of the electrolyte resistance (R_{el}) as a function of ε when the SPE is stretched continuously or stopped time by time. For $\varepsilon \leq 60$ %, there is no difference between the two experimental protocols and R_{el} remains constant until $\varepsilon = 15$ % then increases linearly until 60 %. For higher ε, R_{el} continues to increase in a quasi-linear fashion for the continuous mode while during stop-motion it increases in a more pronounced manner. This is attributed to the local reorganization of the polymer chain where the chains relax between two stretching steps. Indeed, looking at the experimental time as a function of ε in **Figure 7b**, the longer the

relaxation time during stop-motion experiment the higher R_{el}. This is illustrated at ε = 60 % where the deviation of R_{el} from the continuous test (**Figure 7a**) is correlated with a longer relaxation time of about 45 min (**Figure 7b**). To go further, $\sigma_{//}$ was calculated based on eq. 6 using camera picture of the PEO_{5000} at each elongation and the thickness evolution determined from the initial and final one then using eq. 10 for intermediate thicknesses. **Figure 7c** represents $\sigma_{//}$ as a function of ε. For the two types of experiment (continuous *vs.* stop-motion), the initial $\sigma_{//}$ (ε = 0 %) at 60 °C is identical with an average value of 3.80 ± 0.01 10^{-4} $S.cm^{-1}$. This value is comparable with that obtained for the same electrolyte having a parallelepiped shape in an Al symmetric pouch cell (3.84 ± 0.05 10^{-4} $S.cm^{-1}$, see **Figure S7a**). For both experimental modes, $\sigma_{//}$ is identical and increases with ε up to 21 % reaching 4.83 10^{-4} $S.cm^{-1}$, *i.e.* an increase by a factor of about 1.3. This is a rather small factor compared to some literature data where a factor of 3.5 was obtained at 65 °C for a PEO/LiI electrolyte[18] whose ionic conductivity was measured back at room temperature. For 21 % ≤ ε ≤ 60 %, $\sigma_{//}$ is plateauing for both experiments. For 60 % ≤ ε ≤ 125 %, $\sigma_{//}$ remains constant when the SPE is continuously stretched while for the stop-motion experiment $\sigma_{//}$ starts to decrease. Such decrease is correlated with the increase of R_{el} during longer relaxation time. We note that $\sigma_{//}$ tends to return to its initial value if sufficient time is given for the material, *i.e.* the stretched polymer chains return to the relaxed conformation. For ε ≥ 100 %, $\sigma_{//}$ of the stop-motion experiment is even lower than the initial value as the SPE tends to bleed and its geometrical dimensions (length, width, thickness) become hard to determine. To get a better understanding of the PEO_{5000} behavior with elongation, stress-strain experiment was performed under a dry air flow at 60 °C. **Figure S8** shows the resulting stress as a function of ε. The amplitude of the curve and the shape are in relative agreement with literature data.[12,38] For $\varepsilon \leq$ 15 %, the stress increases linearly with ε corresponding to a zone of entropic elasticity of entanglement. It is a pseudo-reversible elastic elongation where the applied force causes a stretching of the entangled polymer chains which correlates with the increase in $\sigma_{//}$ (**Figure 7c**). In this elastic region, the chains tend to be aligned and adopt a fibril-like structure where the cationic and anionic transport can be both favored. Indeed, intrachain transport where the cations move along the polymer chain [7] may be enhanced compared to interchain one, and the poorly solvated anions by the PEO chains [39] may also have an higher conductivity as the elongated chains can better distribute the available free volume leading to more efficient pathways. To go further, adapting our experimental setup to use non-blocking Li electrodes, could help to determine the other transport properties, namely the transference number and the diffusion coefficient, to make a clear distinction between

cationic and anionic transport upon SPE elongation. For 15 % ≤ ε ≤ 46 %, there is a transition between the elasticity zone and the flow zone that appears at about 46 % of elongation up to about 120 %. In this flow zone, the stretched polymer chains tend to slip relative to each other (creeping effect) inducing a drop in the SPE viscosity. In this zone, the local chain dynamic which pilots the ionic transport mechanism may be weakly affected by the slipping effect inducing a constant ionic conductivity. In addition, if there are stops during the SPE stretching in the elastic or flow zone the polymer chains will tend to return to a state close to the initial one as seen in the drop of $\sigma_{//}$ in the stop-motion experiment (**Figure 7c**). At higher ε values, the PEO_{5000} tends to reach the tensile strength. For the next set of measurements, we choose to focus on the continuous elongation technique to investigate the effect of the polymer nature rather than relaxing time between each elongation step.

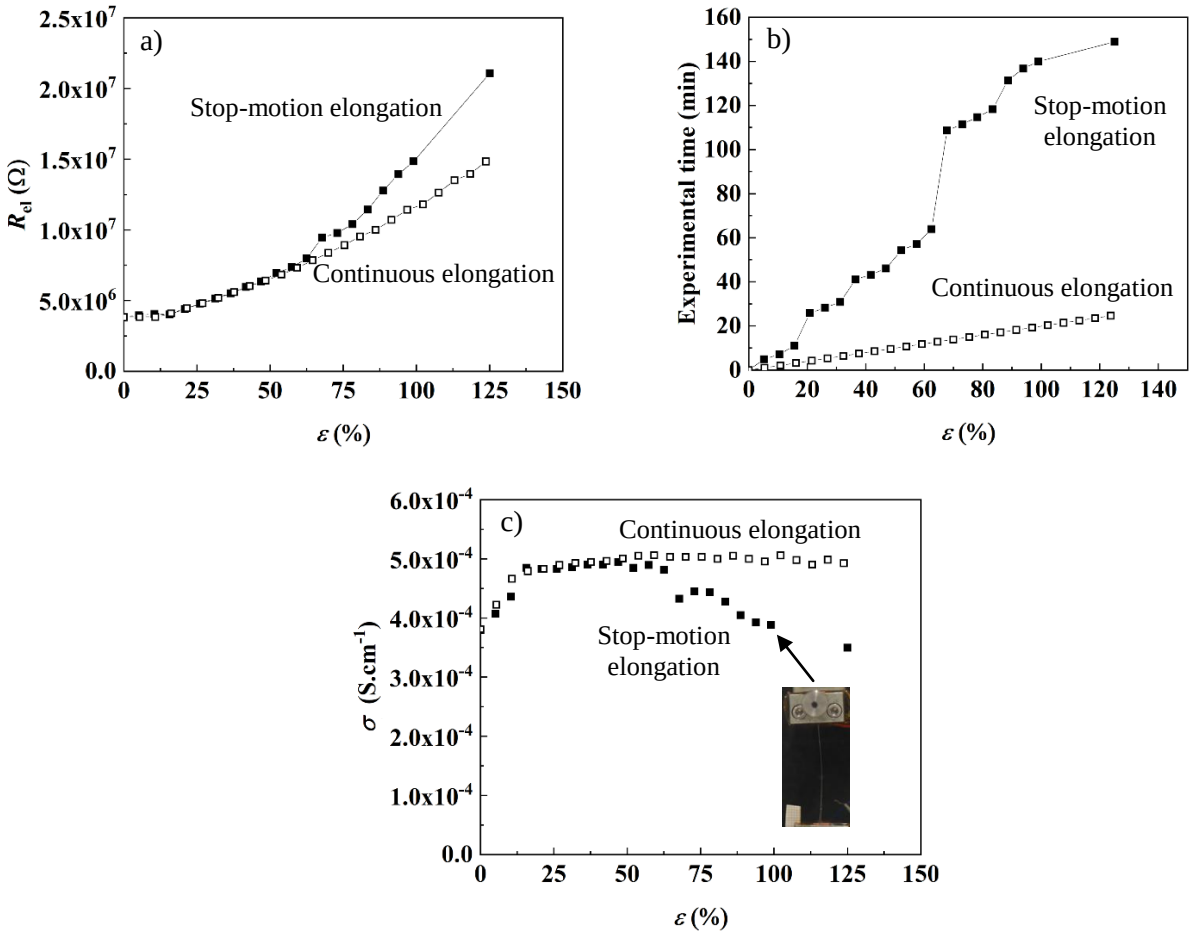

Figure 7. a) Electrolyte resistance (R_{el}) at 60 °C as a function of the elongation (ε) for the PEO_{5000} electrolyte during continuous or stop-motion experiments. The corresponding b) experimental time and c) in-plane ionic conductivity (σ) are displayed as a function of ε.

The $SEO_{20}S\_53$ electrolyte was then investigated at a temperature higher than its T_m, at 61 °C, in the sample environment and under a continuous elongation. The evolution of R_{el} with ε is displayed in **Figure 8a**. R_{el} increases linearly with ε with a transition at 60 % where the slope becomes higher reaching then a value 5 times higher than the initial one after a 114 % elongation. Then, using our methodology, the length (**Figure 8b**), projected surface (**Figure 8c**), average width (**Figure 8d**), and estimated thickness (**Figure 8e**) based on the initial (106 µm), final (65 µm) ones, and using eq. 10 ($\nu = 0.38$) for intermediate values are all displayed as a function of ε. From these results and using eq. 6, $\sigma_{//}$ is shown at the different elongation rates in **Figure 8f**. Note, the initial $\sigma_{//}$ (ε = 0 %) of the $SEO_{20}S\_53$ corresponds to the conductivity measured in pouch cells (see **Figure S7b**). For $\varepsilon \leq 20$ %, contrary to PEO_{5000}, $\sigma_{//}$ remains constant with a value around 9.8 10^{-5} $S.cm^{-1}$ where the SPE is in its elastic zone.[5] This effect may be ascribed to the confinement of the PEO chain due to the presence of the PS block hindering the capability of the PEO chain to fully stretched and thus ionic transport. Indeed, $SEO_{20}S\_53$ is nanostructured adopting a lamellar morphology at the nm length scale.[40] For $20 \leq \varepsilon \leq 80$ %, where $SEO_{20}S\_53$ is typically in its plastic zone[6], $\sigma_{//}$ increases slightly reaching a plateau value in a similar fashion than PEO_{5000} at 1.01 10^{-4} $S.cm^{-1}$. For larger elongation, $\sigma_{//}$ steps up reaching 1.22 10^{-4} $S.cm^{-1}$ at ε = 114 %. Such increase is correlated with the transition observed for R_{el} at ε = 80 % mainly due to a change of the slope in the width with ε (reduction of the width). The experiment could not be performed at higher elongation as the distance between the clamps reached the experimental limit. We tentatively ascribe the observed transition to a reorganization of the SPE grain microstructure[40] with for example alignment of the PS chain domains inducing a lowering of the tortuosity, increasing thus $\sigma_{//}$. Therefore, it would be of interest to perform in situ small-angle X-ray scattering during an elongation test[21] with similar experimental condition. Nevertheless, the overall conductivity gain at 61 °C from ε of 0 % to 114 % is 1.23. This value is in the same modest range as the one obtained for PEO_{5000} (value of 1.3 obtained at 60 °C during continuous elongation, see **Figure 7c**). When the PEO domains are aligned the in-plane ionic transport in nanostructured block copolymer (here $SEO_{20}S\_53$) is like that of a PEO homopolymer electrolyte. The results from PEO_{5000} and $SEO_{20}S\_53$ indicate that for $T > T_m$, mechanical stretching moderately favor $\sigma_{//}$. To go further, it would also be interesting to measure to corresponding through-plane conductivity to get insight on the effective anisotropy[21] when polymer chains are stretched.

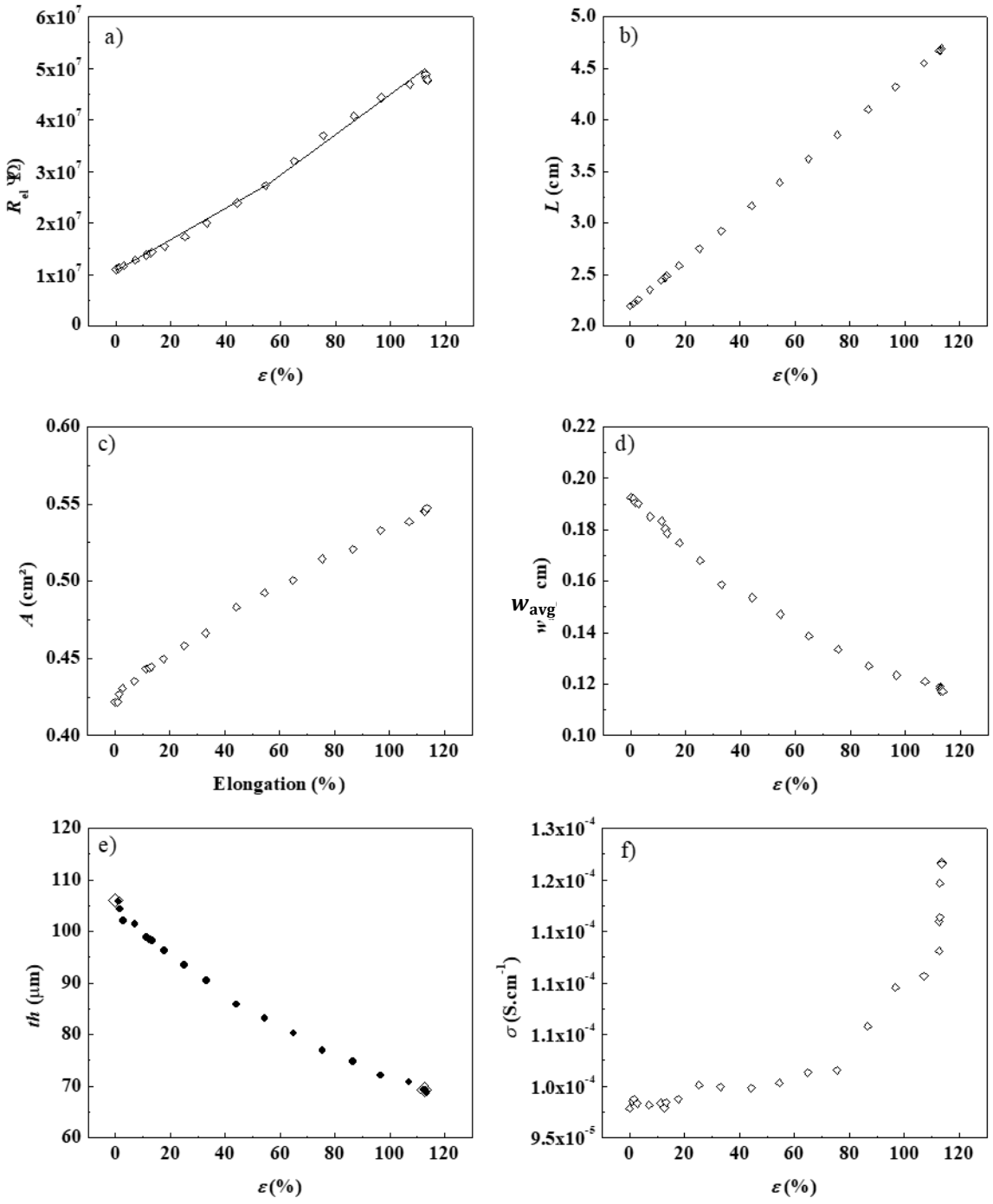

Figure 8. Elongation (ε) of the $SEO_{20}S\_53$ copolymer electrolyte at 61 °C with the a) electrolyte resistance (R_{el}) with the slopes before and after 60 % of elongation indicated as straight lines, b) length (L), c) projected area (A), d) average width (w_{avg}), e) initial and final

(open symbols) and intermediate (eq. 10 with $\nu = 0.38$, black circles) thickness (*th*), and f) in-plane ionic conductivity (σ).

To get insight on the behavior of the electrolyte below T_m, SPEs shaped as a dumbbell were stretched in between 35 and 42 °C. First, results for HySI_20 stretched under continuous elongation at 35 °C are presented in **Figure 9**. The evolution of R_{el} with ε up to 90 % is displayed in **Figure 9a**. Throughout the experiment, the sample remains homogeneous based on the camera pictures which is attributed to the crosslinking, *i.e.* no phase transition. Then, using our methodology, the length (**Figure 9b**), projected surface (**Figure 9c**), average width (**Figure 9d**), and thickness with $\nu = 0.37$ in eq. 10 (**Figure 9e**) were determined as a function of ε. Finally, $\sigma_{//}$ *vs.* ε is shown in **Figure 9f**. Note, the initial $\sigma_{//}$ at ε = 0 % of the HySI_20 at 35 °C matches the pouch cell conductivity (**Figure S7c**). The length and the projected area (and thus w_{avg}) display a linear relationship with ε while the thickness is decreasing according to the empirical power law (eq. 10). Consequently, $\sigma_{//}$ increases quasi-linearly with ε by a factor 2.45 from 5.83 10^{-7} S.cm^{-1} (ε = 0 %) to 1.43 10^{-6} S.cm^{-1} (ε = 90 %) which is almost twice that obtained for the PEO_{5000} and $SEO_{20}S\_53$ electrolytes at 60 °C. Despite the different nature of the HySI_20 electrolyte, being a crosslinked material, the gain in ionic conductivity remains modest. In this experiment, the crosslinked HySI_20 electrolyte [29] remains in its elastic domain over the elongation range. Indeed, after stretching the SPE returns to its initial geometry. Moreover, the HySI_20 being a single-ion conductor, the linear increase of the in-plane conductivity with elongation is attributed to cationic conductivity modification. In single-ion conducting SPE, the gradual enhancement of the cationic transport mechanism with elongation may be correlated with a more efficient intrachain transport. Going to higher ε value would further increase the conductivity and a gain of one decade would require stretching at least up to 600 % without any break. Therefore, highly elastic electrolytes are desired as for example those made of multiblock copolymers comprising poly(tetramethylene oxide) and poly(ethylene terephthalate) that can withstand being stretched up to 600 % [41].

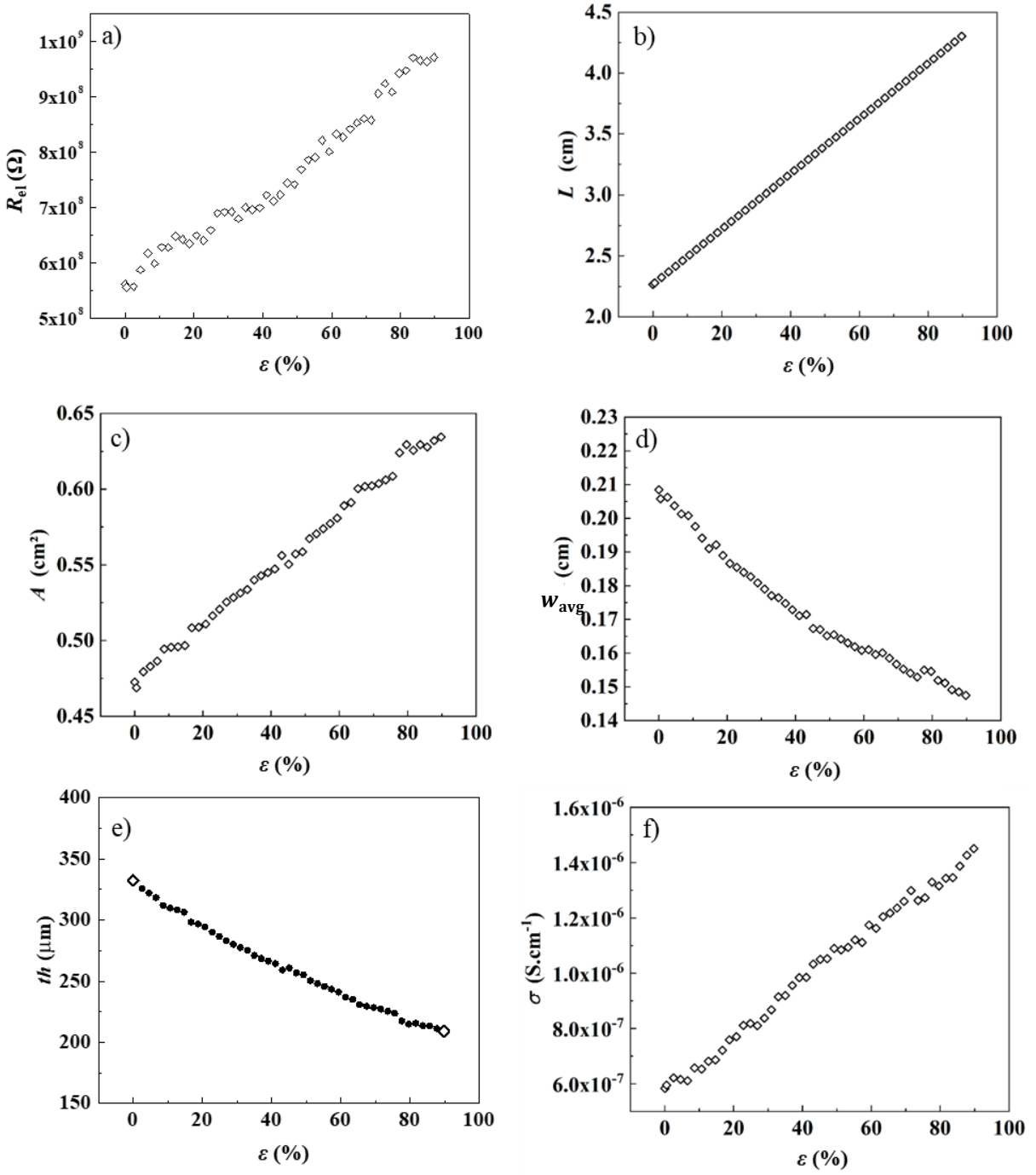

Figure 9. Elongation (ε) of the HySI_20 crosslinked electrolyte at 35 °C with the a) electrolyte resistance (R_{el}), b) length (L), c) projected area (A), d) average width (w_{avg}), e) initial and final (open symbols) and intermediate (eq. 10 with ν = 0.37, black circles) thickness (th), and f) in-plane ionic conductivity (σ).

In another series of experiment, SPEs made of PEO_{5000} were stretched continuously at 1 $mm.min^{-1}$ and at 42 °C ($T < T_m$). As a typical example, the evolution of R_{el} of the PEO_{5000} electrolyte as a function of ε, up to 76 %, is shown in **Figure 10**. In addition, camera pictures of the SPE are shown at selected ε of 0, 9, 11, and 42 %.

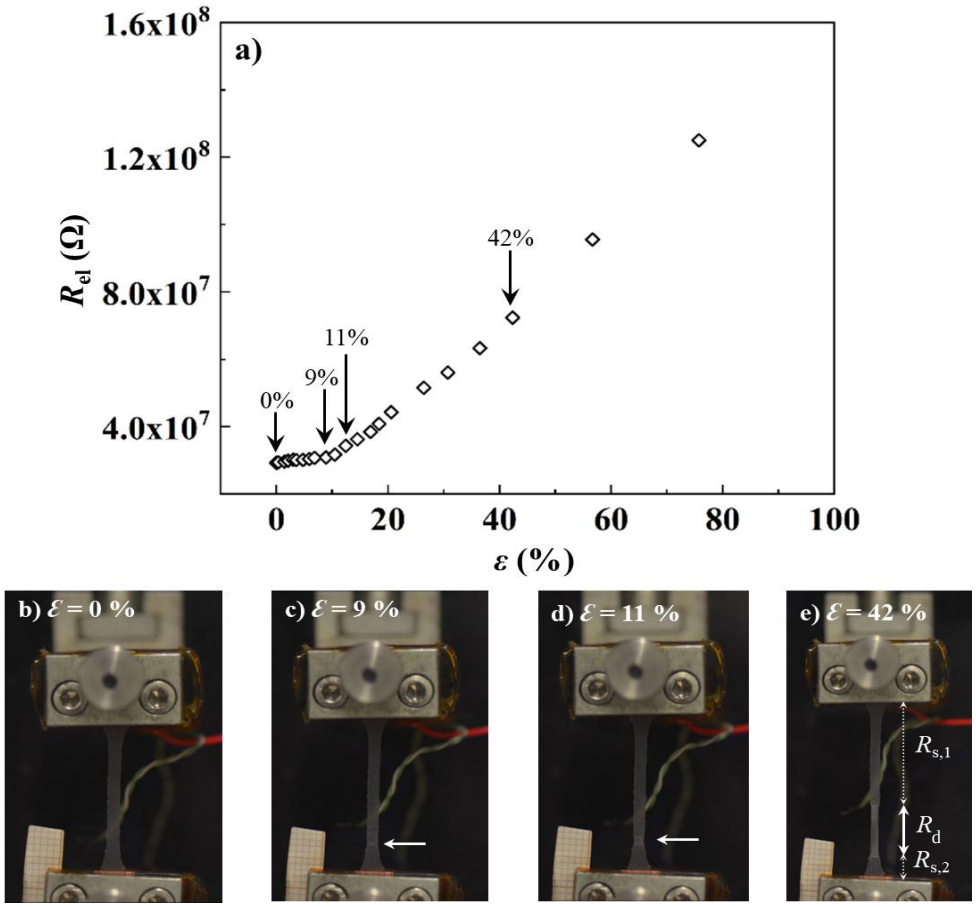

Figure 10. a) Electrolyte resistance (R_{el}) as a function the elongation (ε) of the PEO_{5000} electrolyte at 42 °C, b - e) camera pictures of the electrolyte at selected ε.

Similar to the evolution of R_{el} with ε of the PEO_{5000} at 60°C, R_{el} at 42 °C remains first constant up to 9 % of elongation then starts to increase linearly. For $\varepsilon \leq 9$ %, $\sigma_{//}$ is 2.5 10^{-5} $S.cm^{-1}$ which is in accordance with the in-plane PEO_{5000} conductivity in pouch cell (**Figure S7a**). For $\varepsilon \geq 9$ %, the slope of the linear increase of R_{el} with ε is higher by a factor of 13 than the one at 60 °C. Indeed, at 9 % elongation, a necking region appears having a blurred white color in the lower part of the film as indicated by the arrow in the pictures in **Figure 10c** and **10d**. At higher ε this region tends to expand as illustrated in **Figure 10e** (ε = 42 %). The formation of a neck within the samples corresponds to the beginning of an irreversible deformation [42]. This plastic deformation in semi-crystalline polymer such as PEO involves

large changes within the polymer structure for both the bulk and interfaces of the crystalline regions. The amorphous part of the polymer also changes upon stretching, with a chain alignment [16]. In PEO electrolytes, this domain is only seen for $T < T_m$ and during the stretching of the semi-crystalline polymers as reported in literature by Golodnitsky and coworkers [11]. This result also correlates the work of Gaucher-Miri *et al.*[43] on X-ray scattering performed during the tensile test. They concluded that the necking region resulted from the transformation of the polymer spherulites into fibrillar structures with the presence of interfibrillar microvoids. This new structuration is accompanied by a whitening of the sample (resulting from the presence of the voids that diffuses the light) which is observed as well in the investigated SPEs (see for example **Figure 10e**). To understand its thermodynamical properties, a PEO_{5000} electrolyte was stretched up to ε of 150 % inside a glove box at room temperature and the defect domain was cut and quickly placed in a DSC pan and hermetically sealed. The DSC program was initiated by a cooling scan at 20 °C.min^{-1} down to -100 °C to quench the sample prior performing a heat-cool-heat cycle still at 20 °C.min^{-1}. The thermograms of the defect portion and of a neat PEO_{5000} electrolyte are compared in **Figure 11** for the first and second heating scans. During the first heating scan (**Figure 11a**), the T_g of the defect domain and neat PEO_{5000} are -31.3 °C and -43.8 °C, respectively. These values remain unchanged during the second heating scan (**Figure 11b**) showing the thermodynamical stability of the defect domain. The higher T_g of the defect phase may be ascribed to a salt segregation effect.[44] Indeed, T_g is highly influenced by the salt concentration.[45] For the melting peaks at about 60 °C, during the first heating scan, both melting transitions start at about 42.3 °C and the defect sample presents two endothermic peaks ascribed to two populations of PEO crystallites in accordance with the work of Liu *et al.*[21] During the second heating, the two melting peak starts also at similar values. In addition, the PEO crystallinity index (χ_c) based on eq. 2 of the defect domain during the first heating is 29.2 % which increases up to 34.8 % for the second heating scan remaining below that of the neat PEO (42.4 % for the two heating scans). Therefore, the chain elongation of the PEO homopolymer at $T < T_m$ induces the formation of a necking region made of modified PEO whose T_g is higher and X_c lower than the neat PEO electrolyte. The goal is now to determine the ionic conductivity in this specific region.

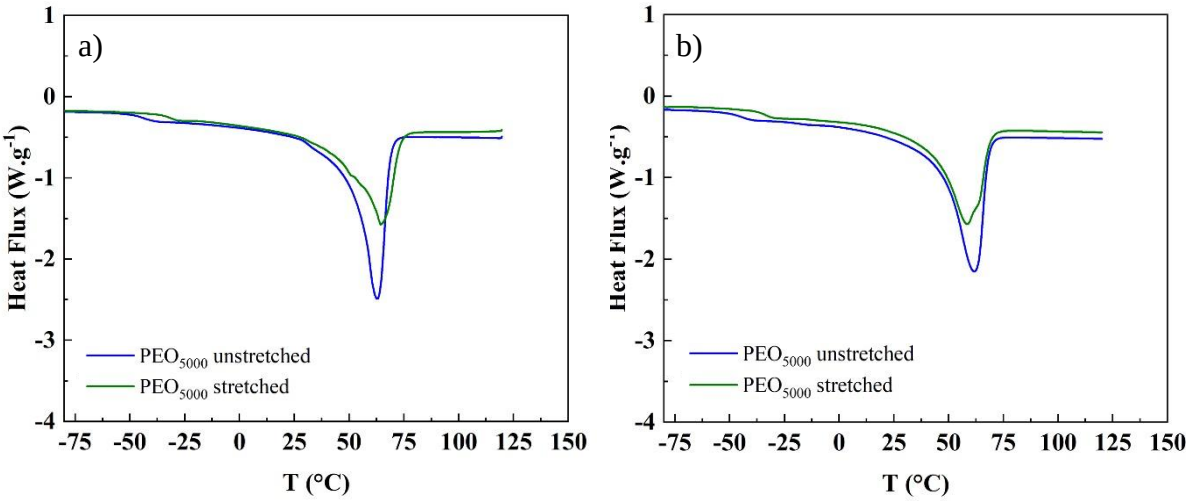

Figure 11. DSC thermograms of the neat PEO_{5000} electrolyte and of the defect region of a 150 % stretched PEO_{5000} at room temperature during the a) first and b) second heating scan.

Because of the appearance of the defect region, the electrolyte film can be decomposed into three domains, two closes to the clamps where the PEO_{5000} chains are stretched of resistances $R_{s,1}$ and $R_{s,2}$ and in between the defect region of resistance R_d. This situation is depicted in **Figure 10e**. Therefore, the electrolyte resistance is:

$$R_{el} = R_{s,1} + R_d + R_{s,2} \quad (11)$$

Each resistance can be expressed as a function of the physical length, width and thickness and respective ionic conductivity at a given elongation. Based on the picture analysis, the evolution of the geometrical dimensions of the stretched and defect regions of the SPE can be determined. Consequently, the evolution of each geometrical dimension of the SPE domains is reported in **Figure 12** as a function of ε using the subscript "s" for the stretched region and "d" for the defect domain. Interestingly, by looking at the top and bottom domains of the stretched PEO_{5000}, their respective dimensions do not evolve much as soon as the defect domain appears (**Figure 12a-d**). This suggests that the chains are stuck in their stretched conformation at 9 %, *i.e.* they have the same conductivity (σ_s). eq. 11 can then be reduced into:

$$R_{el} = R_s + R_d \quad (12)$$

With R_s the sum of the stretched domains ($R_{s,1}$ and $R_{s,2}$) of similar conductivity.

Defining σ_d as the in-plane ionic conductivity of the defect domain, we have:

$$\sigma_{\mathrm{d}} = \frac{1}{R_{\mathrm{el}} - \frac{L_{\mathrm{s}}}{w_{\mathrm{s}}\, th_{\mathrm{s}}\, \sigma_{\mathrm{s}}}} \cdot \frac{L_{\mathrm{d}}}{w_{\mathrm{d}}\, th_{\mathrm{d}}} \qquad (13)$$

In **Figure 12a**, the length of the stretched parts (L_s) remains almost constant at ε = 9 % so the linear increase is only due to the elongation of the defect domain (L_d). Similar behavior is obtained for the projected area (**Figure 12b**) which induces little changes in the average width (eq. 1) for both domains (**Figure 12c**). This implies strong modification of the thickness as seen in **Figure 12d** where the thickness of the stretched domain (th_s) decreases until ε = 9 % and then plateaus in the range of 140 µm while the thickness of the defect domain (th_d) remains constant at about 33 µm. These evolutions and values in thicknesses were confirmed by additional experiments performed on the same PEO_{5000} electrolyte disk (similar initial thickness) that were stretched but stopped at given elongations**.** The thickness of the different domains was then measured with a micrometer without removing the SPE from the clamps. For this, the sample environment was opened to air just for the time of the measurement followed by a drying time of 10 min when closed back. All the samples gave thicknesses of the stretched and defect domains independent of the elongation above ε = 9 %. This indicates that a small portion of the stretched SPE located close to the defect domain is converted into a defective one supplying this domain upon elongation. From this data set, the in-plane conductivity of the stretched domain (σ_s) and of the defect domain (σ_d) are plotted as a function of ε in **Figure 12e**. While σ_s increases slightly between ε = 0 and ε = 9 % by a factor 1.2 from 2.4 10^{-5} $S.cm^{-1}$ to 2.9 10^{-5} $S.cm^{-1}$, as expected for SPE in their elastic zone, then remains constant at higher ε, σ_d quickly stabilizes around 5 10^{-5} $S.cm^{-1}$ independently of ε. σ_d is thus higher than the stretched one by a factor 1.7. This factor is similar to that reported for a PEO/LiI (EO/Li = 40) stretched at room temperature[18] but remains lower than most of the gain reported in literature with electrolytes made of PEO/$LiClO_4$ or PEO/LiTFSI.[19,21]

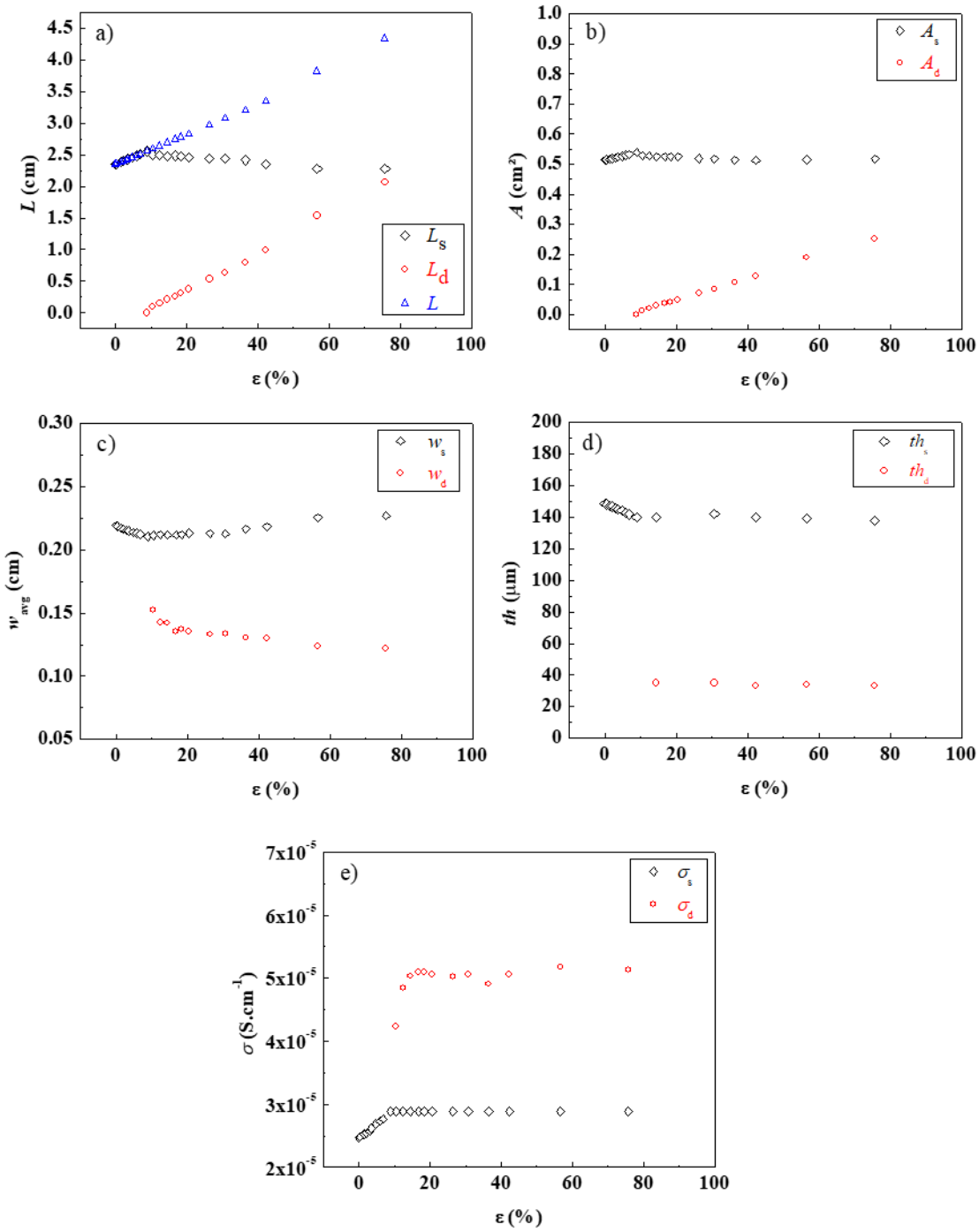

Figure 12. Elongation (ε) of the PEO_{5000} homopolymer electrolyte at 42 °C with the a) length (L), b) projected area (A), c) average width (w_{avg}), d) thickness (th), and e) in-plane ionic conductivity (σ).

The last studied SPE is the nanostructured $SEO_{20}S\_53$ stretched continuously in the sample environment at 35 °C ($T < T_m$). When placed in the sample environment, knowing the sample geometry, $\sigma_{//}$ was determined at 35 °C and the result is presented in **Figure S7b** showing the good agreement with $\sigma_{//}$ from pouch cells during their first heating scan, *i.e.* the sample is not annealed. For completeness, a parallel experiment was performed on an annealed sample where the sample was held at 60 °C for about 30 min in a sealed pouch bag prior being mounted into the sample environment. The resulting conductivity data at 35 °C overlap the one of the pouch cells but during the cooling scan that followed the heating scan. This hysteresis on conductivity is typical of semi-crystalline polymer electrolytes where the kinetic of crystallization during cooling leads to a salt enrichment of the amorphous phase improving thus the ionic conductivity at $T < T_m$.[46,47] As for the previous SPEs, the result of the elongation experiment at 35 °C is presented in **Figure 13** with R_{el}, L, A, w_{avg}, th, and $\sigma_{//}$ as a function of ε. In **Figure 13a**, R_{el} increases from 2.75 10^8 Ω with ε up to 20 % then plateaus for higher elongation with an average value of 3.1 10^8 Ω. This behavior differs from the steadily resistance increased of PEO_{5000} when the defect domain appears (**Figure 10a**). Here, the defect domain appears sooner at about 5 % of elongation which explains the increase of R_{el} with ε. As for PEO_{5000}, the geometrical dimensions of the SPE are decomposed into a defect (subscript d) between stretched (subscript s) domains. In **Figure 13b**, L_d increases linearly with ε when the defect domain appears while the stretched one (L_s) decreases smoothly. This behavior is similar to the PEO_{5000} case. The main difference between the PEO_{5000} and SEO_{20}_53 lies in the evolution of the area of the stretched domain (**Figure 13c**). Indeed, A_s of SEO_{20}_53 decreases with ε while it remains almost constant (slight decrease) for PEO_{5000}. This translates into an average width of the defect domain (**Figure 13d**) that increases rapidly then plateaus after 20 % of elongation. In addition, the thickness (**Figure 13e**) of both domains when they coexist is independent of ε (th_s = 95 µm and th_d = 45 µm) in a similar fashion than PEO_{5000} (th_s = 140 µm and th_d = 33 µm). This implies that little by little portions of the stretched domain (**Figure 13a**) is converted into the defective one where the polymer chains may adopt a given structure weakly dependent of ε possibly piloted by the glassy PS blocks. This induces an in-plane conductivity of the defect domain (σ_d, **Figure 13f**) quasi-independent of ε reaching 8.7 10^{-5} S.cm^{-1}. Interestingly, σ_d is higher than the stretched one (σ_s) by a factor of 18, a decade higher than the factor of comparison obtained for the PEO homopolymer which may be seen as equivalent to a reduction of the tortuosity factor[5],[48] in the defect domain compared to the stretched one.

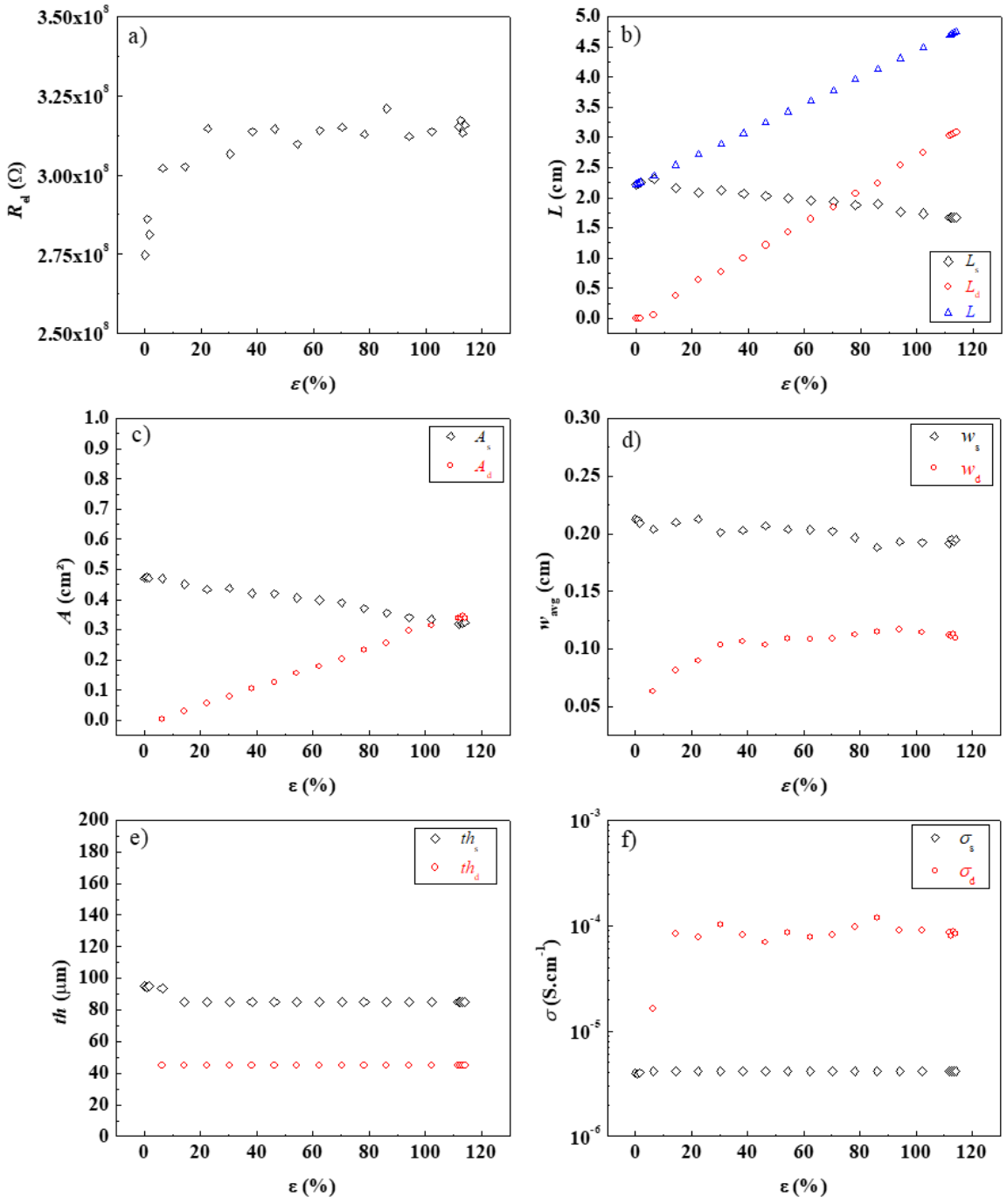

Figure 13. Elongation (ε) of the $SEO_{20}S\_53$ electrolyte at 35 °C with the a) electrolyte resistance (R_{el}), b) length (L), c) projected area (A), d) average width (w_{avg}), e) thickness (th), and f) in-plane ionic conductivity (σ).

4. Conclusion

In this study, we have developed a sample environment dedicated to the coupling of solid polymer electrolyte elongation and impedance measurements in in-plane configuration. The instrument enables to determine accurately the ionic conductivity in temperature and under a dry atmosphere. Various SPEs were investigated depending on their architectures such as PEO homopolymer, nanostructured block copolymer electrolyte, and crosslinked single-ion conducting electrolyte. The developed experimental combines in-situ characterizations (a controlled displacement, and a camera to track the geometrical changes) and geometrical model (to determine the thickness) to accurately follow the changes in the cell constant upon elongation. This is the only possible method to determine the intrinsic material conductivities when the shape is evolving. This protocol was also compared and validated with results from COMSOL simulations.

For the PEO homopolymer the conductivity increases moderately with the elongation for $T > T_m$. This result is actually not very surprising and ascribed to continuous relaxation of the chain elastic domain favoring ionic transport in the in-plane direction. The structure of this material is not changing enough upon stretching to alter its conductivity, and this material can be viewed as a reference to attest the methodology. The resistance changes measured upon stretching are solely related to the geometrical changes, in contrast with the other studied PEO based SPEs. In the case of $SEO_{20}S\_53$ above of the melting temperature, at large elongation an increase in the ionic conductivity is ascribed to material microstructural changes such as PS chain alignment inducing a lower tortuosity. The gain in ionic conductivity is even slightly higher for the crosslinked SPE single-ion conducting electrolyte at $T < T_m$ where the conductivity increases linearly with ε up to 90 % due to a wider elasticity capability. Above T_m, the polymer chains relax rapidly and when stopping the stretching the resistance tends to go back the initial value. Below T_m, the plastic strain may alter permanently the amount and nature of the various phases within the SPE. Both PEO homopolymer and $SEO_{20}S\_53$ block copolymer resulted in significant changes in the electric properties. Within these samples the gain in conductivity is much larger than in the melted state because the morphological changes are more important. This was observed especially for the block copolymer (factor of 18) due to the intrinsic nature of the defect domain which could be made of polymer chains with different thermodynamical properties. This domain can be seen as a conductive domain of different tortuosity. Performing local through-plane conductivity measurements as well as

in-situ SAXS by coupling elongation and impedance experiments would give insight on the effective correlation between local polymer chain deformation and the resulting ionic conductivity (in-plane *vs.* through-plane) to move toward a better understanding of the elongation effect on ionic transport.

5. Declaration of Competing Interest

The authors declare that they have no known competing financial interests or personal relationships that could have appeared to influence the work reported in this paper.

6. Data availability

Data will be made available on request.

7. Acknowledgments

This work is supported by the French National Research Agency in the framework of the "Investissements d'avenir" program (ANR-15-IDEX-02) and under the contract SELPhy (ANR-17-CE05-0032-01). Supplementary material associated with this article can be found, in the online version.

8. References

[1] F. Gebert, M. Longhini, F. Conti, A.J. Naylor, An Electrochemical Evaluation of State-of-the-Art Non-Flammable Liquid Electrolytes for High-Voltage Lithium-Ion Batteries, J. Power Sources 556 (2023) 232412.

[2] J. Lopez, D. G. Mackanic, Y. Cui, Z. Bao, Designing Polymers for Advanced Battery Chemistries, Nat. Rev. Mater. 4 (2019) 312–330.

[3] M.A.S. Azizi Samir, F. Alloin, W. Gorecki, J.-Y. Sanchez, A. Dufresne, Nanocomposite Polymer Electrolytes Based on Poly(oxyethylene) and Cellulose Nanocrystals, J. Phys. Chem. B. 108 (2004) 10845–10852.

[4] H. Ben youcef, O. Garcia-Calvo, N. Lago, S. Devaraj, M. Armand, Cross-Linked Solid Polymer Electrolyte for All-Solid-State Rechargeable Lithium Batteries, Electrochim. Acta. 220 (2016) 587–594.

[5] D. Devaux, D. Glé, T.N.T. Phan, D. Gigmes, E. Giroud, M. Deschamps, R. Denoyel, R. Bouchet, Optimization of Block Copolymer Electrolytes for Lithium Metal Batteries, Chem. Mater. (2015) 4682–4692.

[6] R. Bouchet, S. Maria, R. Meziane, A. Aboulaich, L. Lienafa, J.-P. Bonnet, T.N.T. Phan, D. Bertin, D. Gigmes, D. Devaux, R. Denoyel, M. Armand, Single-ion BAB Triblock Copolymers as Highly Efficient Electrolytes for Lithium-Metal Batteries, Nat. Mater. 12 (2013) 452–457.

[7] A. Maitra, A. Heuer, Cation Transport in Polymer Electrolytes: A Microscopic Approach, Phys. Rev. Lett. 98 (2007) 227802.

[8] M. J. Park, N. P. Balsara, Anisotropic Proton Conduction in Aligned Block Copolymer Electrolyte Membranes at Equilibrium with Humid Air, Macromolecules 43 (2010) 292–298.

[9] D. Golodnitsky, E. Livshits, R. Kovarsky, E. Peled, S. H. Chung, S. Suarez, S. G. Greenbaum, New Generation of Ordered Polymer Electrolytes for Lithium Batteries, Electrochem. Solid-State Lett. 7 (2004) A412-A415.

[10] P. W. Majewski, M. Gopinadhan, W.-S. Jang, J. L. Lutkenhaus, C. O. Osuji, Anisotropic Ionic Conductivity in Block Copolymer Membranes by Magnetic Field Alignment, J. Am. Chem. Soc. 132 (2010) 17516–17522.

[11] D. Golodnitsky, E. Peled, Stretching-Induced Conductivity Enhancement of LiI-(PEO)-Polymer Electrolyte, Electrochim. Acta. 45 (2000) 1431–1436.

[12] T. Kelly, B. M. Ghadi, S. Berg, H. Ardebili, In Situ Study of Strain-Dependent Ion Conductivity of Stretchable Polyethylene Oxide Electrolyte, Sci. Rep. 6 (2016) 20128.

[13] S. Berg, T. Kelly, I. Porat, B. Moradi-Ghadi, H. Ardebili, Mechanical Deformation Effects on Ion Conduction in Stretchable Polymer Electrolytes, Appl. Phys. Lett. 113 (2018) 083903.

[14] D. Golodnitsky, E. Livshits, Y. Rosenberg, E. Peled, S. H. Chung, Y. Wang, S. Bajue, S. G. Greenbaum, A New Approach to the Understanding of Ion Transport in Semicrystalline Polymer Electrolytes, J. Electroanal. Chem. 491 (2000) 203–210.

[15] S. Patra, M. Yeddala, P. Daga, T. N. Narayanan, Anisotropic Mechanical Responses of Poly(Ethylene Oxide)-Based Lithium Ions Containing Solid Polymer Electrolytes, Macromol. Chem. Phys. 220 (2019) 1900348.

[16] L. Flandin, A. Hiltner, E. Baer, Interrelationships between Electrical and Mechanical Properties of a Carbon Black-Filled Ethylene–Octene Elastomer, Polymer 42 (2001) 827–838.

[17] S. H. Chung, Y. Wang, S. G. Greenbaum, D. Golodnitsky, E. Peled, Uniaxial Stress Effects in Poly(ethylene oxide)-LiI Polymer Electrolyte Film: A 7Li Nuclear Magnetic Resonance Study, Electrochem. Solid-State Lett. 2 (1999) 553-555.

[18] D. Golodnitsky, E. Livshits, A. Ulus, Z. Barkay, I. Lapides, E. Peled, S. H. Chung, S. Greenbaum, Fast Ion Transport Phenomena in Oriented Semicrystalline LiI−P(EO)$_n$-Based Polymer Electrolytes, J. Phys. Chem. A. 105 (2001) 10098–10106.

[19] D. Golodnitsky, E. Livshits, E. Peled, Highly Conductive Oriented PEO-based Polymer Electrolytes, Macromol. Symp. 203 (2003) 27–46.

[20] L. Gitelman, M. Israeli, A. Averbuch, M. Nathan, Z. Schuss, D. Golodnitsky, Polymer Geometry and Li+ Conduction in Poly(Ethylene Oxide), J. Comput. Phys. 227 (2008) 8437–8447.

[21] C. Liu, X. Tang, Y. Wang, R. L. Sacci, W. Bras, J. K. Keum, X. C. Chen, Ionic Conductivity Enhancement of Polymer Electrolytes by Directed Crystallization, ACS Macro Lett. 11 (2022) 595–602.

[22] C. M. Burba, L. Woods, S. Y. Millar, J. Pallie, Polymer Chain Organization in Tensile-Stretched Poly(Ethylene Oxide)-Based Polymer Electrolytes, Electrochim. Acta 57 (2011) 165–171.

[23] M. Rosso, C. Brissot, A. Teyssot, M. Dollé, L. Sannier, J. M. Tarascon, R. Bouchet, S. Lascaud, Dendrite Short-Circuit and Fuse Effect on Li/Polymer/Li Cells, Electrochim. Acta 51 (2006) 5334–5340.

[24] J. Schindelin, I. Arganda-Carreras, E. Frise, V. Kaynig, M. Longair, T. Pietzsch, S. Preibisch, C. Rueden, S. Saalfeld, B. Schmid, J.-Y. Tinevez, D.J. White, V. Hartenstein, K. Eliceiri, P. Tomancak, A. Cardona, Fiji: an Open-Source Platform for Biological-Image Analysis, Nat. Methods 9 (2012) 676–682.

[25] R. Jeanne-Brou, J. Deseure, T. Phan, R. Bouchet, D. Devaux, Anisotropic Ionic Transport Properties in Solid PEO Based Electrolytes, Electrochim. Acta 434 (2022) 141268.

[26] A. Michel, Polymer Solid Electrolytes - an Overview, Solid State Ion. 9–10 (1983) 745–754.

[27] F. Croce, G. B. Appetecchi, L. Persi, B. Scrosati, Nanocomposite Polymer Electrolytes for Lithium Batteries, Nature 394 (1998) 456–458.

[28] B. Kumar, S. Koka, S. J. Rodrigues, M. Nookala, Physical Aging Effects on Conductivity in Polymer Electrolytes, Solid State Ion. 156 (2003) 163–170.

[29] S. Issa, R. Jeanne-Brou, S. Mehan, D. Devaux, F. Cousin, D. Gigmes, R. Bouchet, T.N.T. Phan, New Crosslinked Single-Ion Silica-PEO Hybrid Electrolytes, Polymers. 14 (2022) 5328.

[30] M. Watanabe, H. Tokuda, S. Muto, Anionic Effect on Ion Transport Properties in Network Polyether Electrolytes, Electrochim. Acta. 46 (2001) 1487–1491.

[31] I. Szabo, L.I. Scurtu, H. Raboca, F. Mariasiu, Topographical Optimization of a Battery Module Case That Equips an Electric Vehicle, Batteries. 9 (2023) 77.

[32] D. Devaux, R. Bouchet, D. Glé, R. Denoyel, Mechanism of Ion Transport in PEO/LiTFSI Complexes: Effect of Temperature, Molecular Weight and End Groups, Solid State Ion. 227 (2012) 119–127.

[33] R. Bouchet, S. Lascaud, M. Rosso, An EIS Study of the Anode Li/PEO-LiTFSI of a Li Polymer Battery, J. Electrochem. Soc. 150 (2003) A1385-A1389.

[34] L. O. Griffin, Physical Constants of Linear Homopolymers, Vol. 12, Springer Science & Business Media (2012).

[35] S. Gao, W. Liu, L. Zhang, A. K. Gain, A New Polymer-Based Mechanical Metamaterial with Tailorable Large Negative Poisson's Ratios, Polymers. 12 (2020) 1492.

[36] H. S. Cho, H. A. Kim, D. W. Seo, S. C. Jeoung, Poisson's Ratio Measurement Through Engraving the Grid Pattern Inside Poly(dimethylsiloxane) by Ultrafast Laser, Jpn. J. Appl. Phys. 60 (2021) 101004.

[37] G. Zardalidis, E. Ioannou, S. Pispas, G. Floudas, Relating Structure, Viscoelasticity, and Local Mobility to Conductivity in PEO/LiTf Electrolytes, Macromolecules 46 (2013) 2705–2714.

[38] K. Zhu, Y. Liu, J. Liu, A Fast Charging/Discharging All-Solid-State Lithium Ion Battery Based on PEO-MIL-53(Al)-LiTFSI Thin Film Electrolyte, RSC Adv. 4 (2014) 42278–42284.

[39] J. Chattoraj, M. Knappe, A. Heuer, Dependence of Ion Dynamics on the Polymer Chain Length in Poly(ethylene oxide)-Based Polymer Electrolytes, J. Phys. Chem. B 119 (2015) 6786–6791.

[40] R. Bouchet, T.N.T. Phan, E. Beaudoin, D. Devaux, P. Davidson, D. Bertin, R. Denoyel, Charge Transport in Nanostructured PS–PEO–PS Triblock Copolymer Electrolytes, Macromolecules. 47 (2014) 2659–2665.

[41] B. Zhao, L. Ma, H. Xie, K. Wu, X. Wang, S. Huang, X. Zhu, X. Zhang, Y. Tu, J. Chen, Self-adaptive Multiblock-Copolymer-Based Hybrid Solid-State Electrolyte for Safe and Stable Lithium-Metal Battery, Electrochim. Acta. 371 (2021) 137702.

[42] Y. Tomita, Simulations of Plastic Instabilities in Solid Mechanics, Applied Mech. Rev. 47 (1994) 171–205.

[43] V. Gaucher-Miri, P. François, R. Séguéla, On the Mechanisms of Initiation and Propagation of Plastic Instability in Polyethylene Under Tensile Drawing, J. Polym. Sci. Part B: Polym. Phys. 34 (1996) 1113–1125.

[44] W.-S. Young, T. H. Epps, Salt Doping in PEO-Containing Block Copolymers: Counterion and Concentration Effects, Macromolecules. 42 (2009) 2672–2678.

[45] S. Lascaud, M. Perrier, A. Vallee, S. Besner, J. Prud'homme, M. Armand, Phase Diagrams and Conductivity Behavior of Poly(ethylene oxide)-Molten Salt Rubbery Electrolytes, Macromolecules 27 (1994) 7469–7477.

[46] S. A. Mullin, A. A. Teran, R. Yuan, N. P. Balsara, Effect of Thermal History on the Ionic Conductivity of Block Copolymer Electrolytes, J. Polym. Sci. Part B: Polym. Phys. 51 (2013) 927–934.

[47] M. Marzantowicz, F. Krok, J. R. Dygas, Z. Florjańczyk, E. Zygadło-Monikowska, The Influence of Phase Segregation on Properties of Semicrystalline PEO:LiTFSI electrolytes, Solid State Ion. 179 (2008) 1670–1678.

[48] G. Jo, O. Kim, H. Kim, U. Hyeok Choi, S.-B. Lee, M. Jeong Park, End-functionalized Block Copolymer Electrolytes: Effect of Segregation Strength on Ion Transport Efficiency, Polym J. 48 (2016) 465–472.